Science of the Total Environment 904 (2023) 167256

Contents lists available at ScienceDirect

Science of the Total Environment

journal homepage: www.elsevier.com/locate/scitotenv

Investigations on microplastic infiltration within natural riverbed sediments

Mirco Mancini *, Simona Francalanci, Lorenzo Innocenti, Luca Solari

Department of Civil and Environmental Engineering, University of Florence, Via S. Marta 3, 50139 Florence, Italy

HIGHLIGHTS

- The relationship between the sediment size and the microplastic (MP) size is a key parameter for MP infiltration.
- MPs in the size range between 0.5-5mm are likely retained in fine and medium gravel layers.
- PET spheres tend to reach greater infiltration depths.
- In deep infiltration the shortest axis of MP particles comes to be the characteristic diameter perpendicular to the motion.

GRAPHICAL ABSTRACT

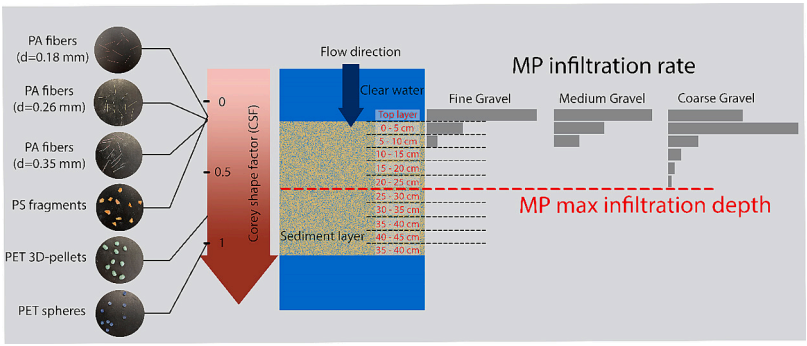

ARTICLE INFO

Editor: Damia Barcelo

Keywords:
Microplastic infiltration
Microplastic retention
Particles properties
Hyporheic zone
Porous media
Riverbed sediment

ABSTRACT

Several studies focused on the role of rivers as vectors of microplastics (MPs) towards the sea. It is well known that during their path through the fluvial environment, MPs interact with riverbed sediments; however, the main factors impacting the mobility of MPs within the upper part of the hyporheic zone are not clear yet. The present work investigates the role of different sediment size layers in affecting the mobility of the most common MP (Polyethylene terephthalate - PET - spheres, PET 3D-ellipsoids, polystyrene - PS - fragments and polyamide - PA - fibers) within sediment porous media under different hydraulic loads (H_L) and time scales (t) conditions. Results indicated the relationship between the characteristic MP diameter and that of the grains as the main parameter for the MP infiltration into the sediment layer. The maximum infiltration depth was found to not depend on H_L and t. However, H_L was able to influence the percentage of MPs penetrating the superficial layer and their distribution within the first 10–15 cm of the sediment layer. None of the MPs were found at depths >20–25 cm, where only PET spheres were detected. Starting from the suffusion theory, a model able to predict the MP maximum infiltration depth in the range of parameter values was provided.

The outcome indicates the importance of considering geometrical and hydrodynamic aspects of the riverbed sediment layer to better characterize the spatial and temporal scales of MP transport in freshwater environments.

* Corresponding author.
E-mail address: mirco.mancini@unifi.it (M. Mancini).

https://doi.org/10.1016/j.scitotenv.2023.167256
Received 3 August 2023; Received in revised form 18 September 2023; Accepted 20 September 2023
Available online 21 September 2023

1. Introduction

The fact that rivers play a key role in transporting plastic debris towards the oceans is widely recognized by the scientific community (Gasperi et al., 2014; Morritt et al., 2014; Schmidt et al., 2017; Lebreton et al., 2017; Meijer et al., 2021). The dynamics of transport and accumulation of plastic debris in aquatic environments are mainly affected by their characteristics, i.e., density, size, and shape (Schwarz et al., 2019; Francalanci et al., 2021) but also by hydrodynamic conditions (e.g., flow velocity, water level and laminar or turbulent flow conditions) (Kumar et al., 2021). Thick-walled, larger plastic debris, constituted by low-density polymers, is usually transported in floating conditions by the rivers directly to the oceans (Schwarz et al., 2019). While for all other cases, recent studies showed that most of the plastic entering the river systems is deposited on riverbanks and floodplains, or retained by in-channel structures (e.g., weirs, dams, and bridges), riverbed sediments and vegetation, determining a long residence time (Kukkola et al., 2023; van Emmerik et al., 2022; Dhivert et al., 2022). Microplastics (MPs), widely defined as plastic particles of a medium size <5 mm (Hidalgo-Ruz et al., 2012; Razeghi et al., 2021), represent the most interesting size class for the abovementioned retention processes. Their size facilitates dispersion and transport, resulting in greater difficulty in retaining them, such as in wastewater purification systems (Becucci et al., 2022; Magni et al., 2019). As a result, these particles likely remain stored in river sediments and interact often with the freshwater biota (Colomer et al., 2019), becoming suitable as vectors to transport pollutants (Alimi et al., 2018).

Recently, the hyporheic zone, defined as the region of the streambed pore water that exchanges with the open water column of rivers (Boano et al., 2014), has been considered in studying MP abundance through field observations. This zone is particularly interesting as it represents pathways for small particle retention (Jiang et al., 2023).

The latest studies on European rivers' sediments found between 18 (Rodrigues et al., 2018) and 70,600 (Hurley et al., 2018) particles per kilogram of sediments, while a concentration of593 particles per kilogram of sediments were found on river floodplains according to Scheurer and Bigalke (2018). In African streambed sediment, Toumi et al. (2019) identified between 2340 and 6920 particles/kg. Ghinassi et al. (2023) collected several sediment samples on alternate bars and riverbanks of the Arno River (Italy). Their results showed a concentration of MPs that ranged between 440 and 5680 particles/kg of sediment; the authors' conclusion for the Arno River was that sinking MPs can be directly incorporated by fine sediment while they are moving to the bottom of the river or indirectly retained by gravel cavities during recessional flood stages. Moreover, Frei et al. (2019) analyzed MPs in the size range 0.5–5 mm in five freeze cores extracted from the Red Main River sediments (Germany): their observations showed detectable MP down to a depth of 0.6 m.

However, most studies are not comparable due to a significant number of variables (i.e., sampling location, sampling method, analysis method) giving a wide range of MP concentrations, as shown by Scherer et al. (2020). In addition, the hydrodynamics of the hyporheic exchange can affect MP retention time by producing changes in their physical and chemical properties due to processes of degradation, fragmentation, and biofouling. This results in an underestimation of the amount of MPs in mass balance models that do not consider the hydrodynamics of the hyporheic zone, as demonstrated by Drummond et al. (2020).

The use of numerical simulation could help in studying the role of the hyporheic zone in trapping MPs. Using this approach, Drummond et al. (2022) simulated the MP accumulation in riverbed sediment via hyporheic exchange from headwaters to mainstems. Their results highlighted the importance of riverbed sediment as a long-term sink (up to 7 years/km) for MPs, about 3 to 8 % of the total mass entering the system each kilometer. At the same time, the remaining 92 to 97 % of the inputs are stored in the riverbed sediment for shorter periods only (0.2 to 0.6 years/km) before being remobilized and transported downstream. However, developing models for the MP infiltration inside porous media, especially when they have particular shapes that differ greatly from the spherical one (for example, fibers and 2D fragments), can be challenging and requires experimental studies to validate and improve the models themselves (Engdahl, 2018).

Hyporheic zones are extremely important as they represent the connection between surface water and groundwater. In their work, Viaroli et al. (2022) concluded that only a few studies concerning MPs are focused on groundwater systems, and they suggest the importance of considering sediment characterization to obtain a good assessment of the MP amount in the subsoil. In addition, it is demonstrated that MPs play an important role in transporting different types of sediment-dwelling pollutants (Wang et al., 2021b; Selvam et al., 2021). Moreover, the MPs themselves can release pollutants due to the presence of components added during the production phase to improve their physical and chemical performance (Bradney et al., 2019). Therefore, studying the MP mobility within the hyporheic zone can be extremely useful for groundwater quality assessment.

Ling et al. (2022), using a physically simulated hyporheic zone, explored the effects of hydrodynamic factors and fluid physicochemical properties (i.e., salinity and temperature) on the transport and retention of polystyrene nano plastics (PSNPs) in a sand porous media. They showed that high salinity conditions reduce the nano plastics infiltration rate due to the strong colloidal attraction and adhesion between PSNPs and sand. They concluded that freshwater systems with low salinity and high flow rate represent the potential conditions for a high MP concentration. Waldschläger and Schüttrumpf (2020) investigated the infiltration behavior of different microplastic particles using glass spheres to simulate natural sediments. They showed that the shape of the plastic particles and the ratio between their size and the size of the sediments are the two main factors that determine the MP infiltration depth. They concluded that the transferability of the glass spheres experiments to natural sediment, as well as time-dependent infiltration, must be investigated.

The present study was designed to provide further information on the dynamics of MP infiltration in natural sediments. A series of laboratory experiments were performed to highlight the main parameters controlling the phenomenon, particularly focusing on the role of: (i) the sediment size, (ii) the MP characteristics (i.e., size, shape, and polymer type), (iii) the hydraulic conditions, and (iv) the time scale of the process.

The experimental setup and the adopted methods of analysis are described in detail. A critical comparison was made both with similar works and with the results from field sampling and a physical interpretation of the findings, considering both hydrodynamics and geometric aspects, starting from the theory of suffusion processes. Finally, we also discussed the importance of this study to better characterize the spatial and temporal scales of MP transport in freshwater environments and the contribution it could provide to developing more efficient MP mass balance models.

2. Materials and methods

2.1. Theoretical background

According to the Darcy theory for an incompressible fluid flowing in a porous media, the hydraulic conductivity (k) can be calculated from the following law:

$$v = ki \tag{1}$$

where v is the mean apparent flow velocity within the porous media, and $i = \Delta/L$ is the hydraulic gradient given by the ratio between the piezometric difference (Δ) and the distance between the two measuring points.

The Corey Shape Factor (CSF) was used to characterize MP geome-

try. The CSF is a dimensionless shape factor representing the relative flatness of the particle, defined as in Eq. (2):

$$\mathrm{CSF} = \mathrm{c} \Big/ \sqrt{ab} \tag{2}$$

where a [m] and b [m] represent the maximum and intermediate axis of particle and c [m] corresponds to the particle's thickness (Albar, 2000). CSF ranges from 0 to 1, with the smaller CSF corresponding to a thinner and flatter particle.

The infiltration process of MPs in the porous layer is described following the suffusion theory (Marot and Benamar, 2013), according to which the soils are schematized as a network of parallel capillary tubes with a constant radius r [m] (Khilar et al., 1985). The radius r was estimated assuming spherical grains and considering r as the mean value of the two inscribed circumferences in the void area when the grain arrangement maximizes or minimizes the volume of the voids themselves.

According to the above theory, there is a need to distinguish between the *initiation of filtration* (particles approaching the soil pores and moving downwards from the surface layer w) and *deep filtration* (particles moving inside the porous medium and depositing at different depths). The efficiency of both processes depends on two categories of parameters: geometrical parameters (i.e., porosity of the porous medium, size and shape of grains composing the porous medium and size, shape, and density of infiltrating particles) and hydraulic parameters (i.e., flow velocity, Reynolds number and Hydraulic gradient). Consequently, two are the main criteria used to evaluate the particles' infiltration capacity: (I) the relationship between the characteristic diameter of grains and that of the particles (geometric criterion); (II) the relationship between the critical hydraulic shear stress produced by the flow and the inertial force of the particles (hydraulic criterion).

Following the hypothesis of Reddi et al. (2000) stating that the hydraulic load governing the suffusion is shear stress, the drag force (F_D) developed along the superficial area of the capillary tubes was calculated:

$$F_D = 1.414 \bullet i \bullet \sqrt{\frac{K_i}{n}} \bullet 2\pi \bullet r \bullet L \tag{3}$$

where i [−] is the hydraulic gradient, L is the length of the internal tube cavities, K_i [m^2] is the intrinsic permeability and n [−] represents the porosity of the soil.

The inertial force (F_i) was expressed as suggested by Marot and Benamar (2013):

$$F_i = V \bullet (\rho_{MP} - \rho) \bullet \frac{U^2}{d_g} \tag{4}$$

where V [m^3] is the measured volume of the MP particles, ρ [kg/m^3] and ρ_{MP} [kg/m^3] are the water density and the MP density, respectively, U [m/s] is the average interstitial flow velocity and d_g [m] represents the D_{50} of the soil. From Eqs. (3) and (4) follows that the relationship F_D/F_I assumes the meaning of a balance between the resistant forces and the driving forces exerted by the flow. Therefore, MP mobility and especially the maximum infiltration depth (I_{DEPTH_MAX}) within saturated porous media is expected to depend on both the physical characteristics and the hydrodynamical forces of the MPs:

$$I_{DEPTH\_MAX} = f(d_{MIN}, F_D, F_I) \tag{5}$$

2.2. Theoretical assumptions on the characteristic MP lengths in the infiltration process

Experiments in a water column demonstrated that MPs with different shapes tend to settle showing different characteristic lengths (Goral et al., 2023; Khatmullina and Isachenko, 2017). Specifically, for most 3D particles, the characteristic length is their maximum or normal diameter being the maximum and the minimum axes of the same order of magnitude; fibers tend to settle with the maximum axis perpendicular to the settling direction; thus, their characteristic length is expected to be the d_{MAX}. Finally, flat fragments tend to settle with their largest projection area normal to the predominant line of motion resulting again in the d_{MAX} as characteristic length. Nevertheless, processes regulating particles settling in a water column and within porous media differ.

Considering the processes of initial filtration and deep filtration, it is useful to highlight several differences. We have assumed MP particles to be rigid. After locating all the MPs lying on the surface of the sediment layer at the initial observation time (t_0) of the infiltration process, we shall consider a single MP particle coming close to a sediment pore. If subjected to vertical forces only, this particle will tend to enter the pore exposing its maximum axis, thus minimizing the moment of inertia (Fig. 1). As a result, investigating the initiation of filtration, the proper MP characteristic diameter to be considered is the particle's maximum diameter (d_{MAX}). However, once the particle has already entered the porous medium (deep filtration), the geometrical pore conditions and the flow forces will induce the particle to rotate with its minimum diameter (d_{MIN}) perpendicular to the direction of the motion; consequently, for deep filtration, the characteristic diameter comes to be d_{MIN}.

2.3. Experimental setup

The experimental setup was designed and built to investigate the infiltration capacity and the mobility of MP into riverbed sediments under different flow conditions (Fig. 2). A transparent plexiglass tank with a section of 0.5 m × 0.5 m × 1 m height was assembled and filled in its middle part with a 0.5 m-thick sediment layer, mimicking the surface layer of the riverbed. A steel grid was fixed 0.25 m from the bottom of the tank to sustain the sediment layer, and a nonwoven fabric layer was added to straighten the outflow and prevent the formation of preferential paths. The tank was filled with clear water above and below the sediment layer, and it was equipped with an inlet and an outlet tap to allow the recirculation of the water flow pumped from a second tank using a submersible pump. A flowmeter (FCH-midi-POM ®RIELS coupled with the 24 V NI9422 acquisition board and acquisition data software ®LabVIEW 2015) was installed at the system's inlet to measure the entering flow discharge throughout the time intervals of the experiment. In order to pressurize the system, an airtight lid was used, and two column piezometers were installed in the water column below and above the sediment layer (0.25 cm and 0.8 m from the bottom of the tank, respectively) to collect data about the hydraulic load conditions and to estimate pressure drops.

2.4. Sediments and MP characterization

In order to simulate the superficial layer of the hyporheic zone, fluvial sediments were taken from a dredge, washed, and sieved to sort them into three different ranges. Following Wentworth's (1922) classification, the three substrates were obtained in the range of coarse gravel (CG, D_{50} = 15.40 mm), medium gravel (MG, D_{50} = 9.45 mm) and fine gravel (FG, D_{50} = 5.05 mm); these three sediments resulted to be well sorted (FG with σ = 0.37, and MG with σ = 0.43) and very well sorted (CG with σ = 0.22), respectively, according to standard deviation (Folk and William Ward, 1957). The effective porosity was measured three times for each sediment type, resulting in 40.30 ± 1.17 %, 43.10 ± 3.87 % and 45.80 ± 1.07 % for FG, MG, and CG, respectively (Table S2). The MP particles selected for the experiments ranged across different sizes, shapes, and densities to explore the effects of these characteristics on infiltration capacity: four different types of MP in a size range between 0.57 mm and 4.43 mm (considering equivalent spherical diameter D_n), with known density, were used (Polyethylene terephthalate - PET - spheres, PET 3D-pellets, polystyrene - PS - fragments, polyamide – PA – fibers having three different diameters), thus resulting in a total number of six samples of MPs used in the experiments(Table S1). Spheres, 3D-

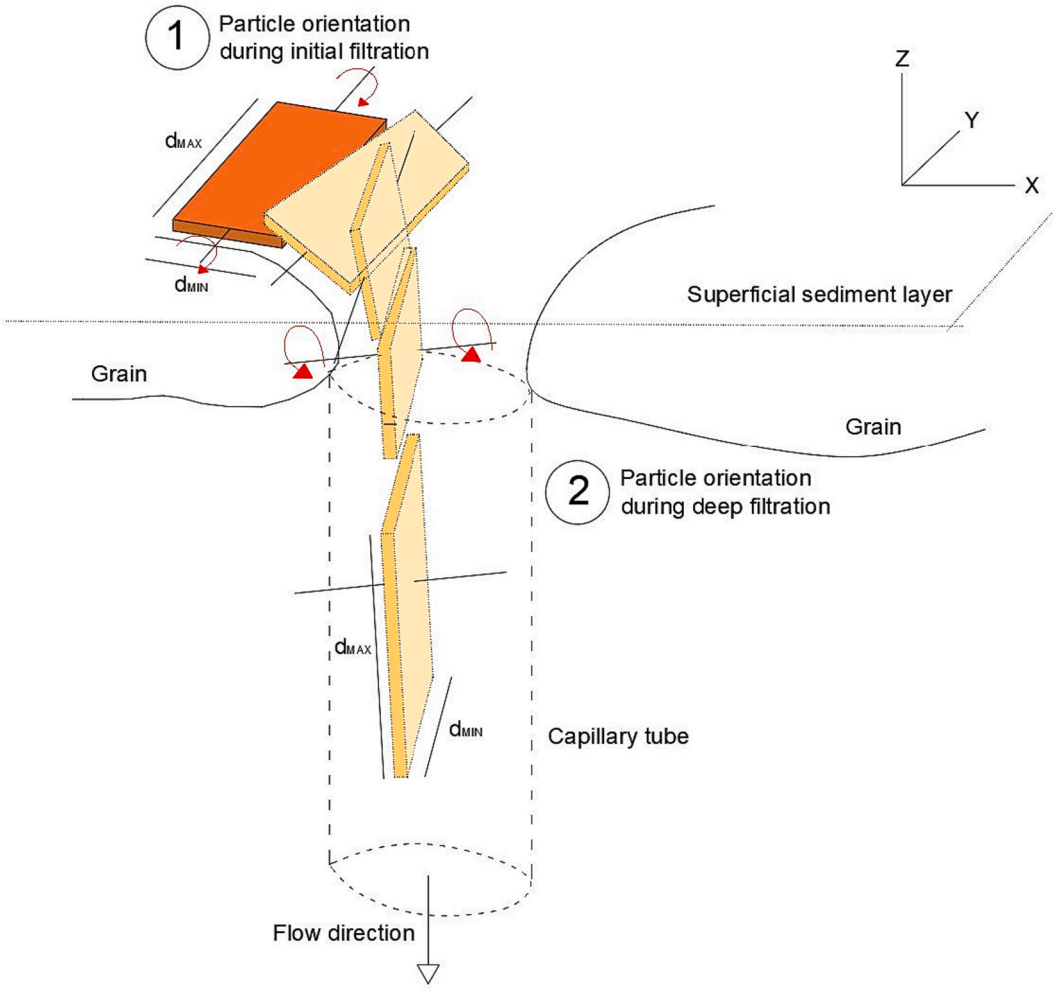

Fig. 1. Scheme of the two infiltration processes (initial and deep filtration) in the case of flat fragments.

pellets, and fragments were purchased ready to use from a manufacturing company, PA fibers were instead prepared by cutting fishing lines of three different diameters (0.18 mm, 0.26 mm, and 0.35 mm). The longest, intermediate, and shortest axis of ten particles for each type of MP were measured using a Vernier gauge and the Image-J software. These subsamples were assumed to represent the whole bulk samples, and the average values were used to calculate the equivalent spherical diameter (D_n) and the Corey shape factor (CSF).

2.5. Experimental procedure

For each experimental run, a quantity of 0.125 m^3 of dry sediments was introduced into the tank paying attention to properly arranging them to obtain a flat surface at the top of the sediment layer. Sediments were previously washed to remove fine particulate and organic matter. Subsequently, the tank was filled with water from the bottom upwards to prevent the formation of air bubbles. Once the sediment layer was completely saturated, the water flow was stopped, and the MP samples were randomly positioned on the surface of the sediment layer, avoiding the areas closer to the plexiglass walls to reduce the possibility of preferential infiltration paths at the corners and the effects of plexiglass edge. Additionally, all MPs were previously wetted to remove the surface tension effect. At the end of each run, the water was released very slowly not to affect the experiment.

Four different hydraulic load conditions (H_L) were considered: 0.25 m, 0.65 m, 0.8 m, and 1 m. In the case of $H_L = 0.25$ m, after the positioning of the plastics, the water level was raised very slowly to the upper edge of the tank without the need to pressurize the system. In the other three cases, it was necessary to seal the tank with the lid and pressurize the system to the desired H_L. The hydraulic load was fixed from the beginning to the end of each run.

The beginning of the experiment was assumed to be when the hydraulic load H_L was reached. From that moment, two different duration times (t) were considered: 1 h and 5 h for each type of sediment layer, (Table 2) and for each type of H_L, for a total of 16 different runs performed (Table 1).

Two experimental configurations were repeated three times (5.1, 5.2, 5.3 and 12.1, 12.2, 12.3), and then the Kruskal-Wallis ANOVA test was used to verify the repeatability (Tables S3 and S4). Once the tank was emptied of the water, all MPs still visible on the surface of the sediment layer were counted and classified as "undisturbed MPs". Then, the sediments were manually removed from the surface to the bottom in 5 cm layers at a time. For every 5 cm-deep layers, MPs were counted by visual observation with the help of a UV light to identify them more easily. The procedure was repeated until the number of particles found equaled the entered amount.

2.6. Data analysis

Data analysis was performed employing the basic Microsoft Excel® (Microsoft, US) function for the calculation of mean values (function "MEAN") and the standard deviation of mean values (function "DEV. ST"). Error bars were calculated using the standard deviation of the mean values. In addition, the linear fit analysis, the power fit analysis

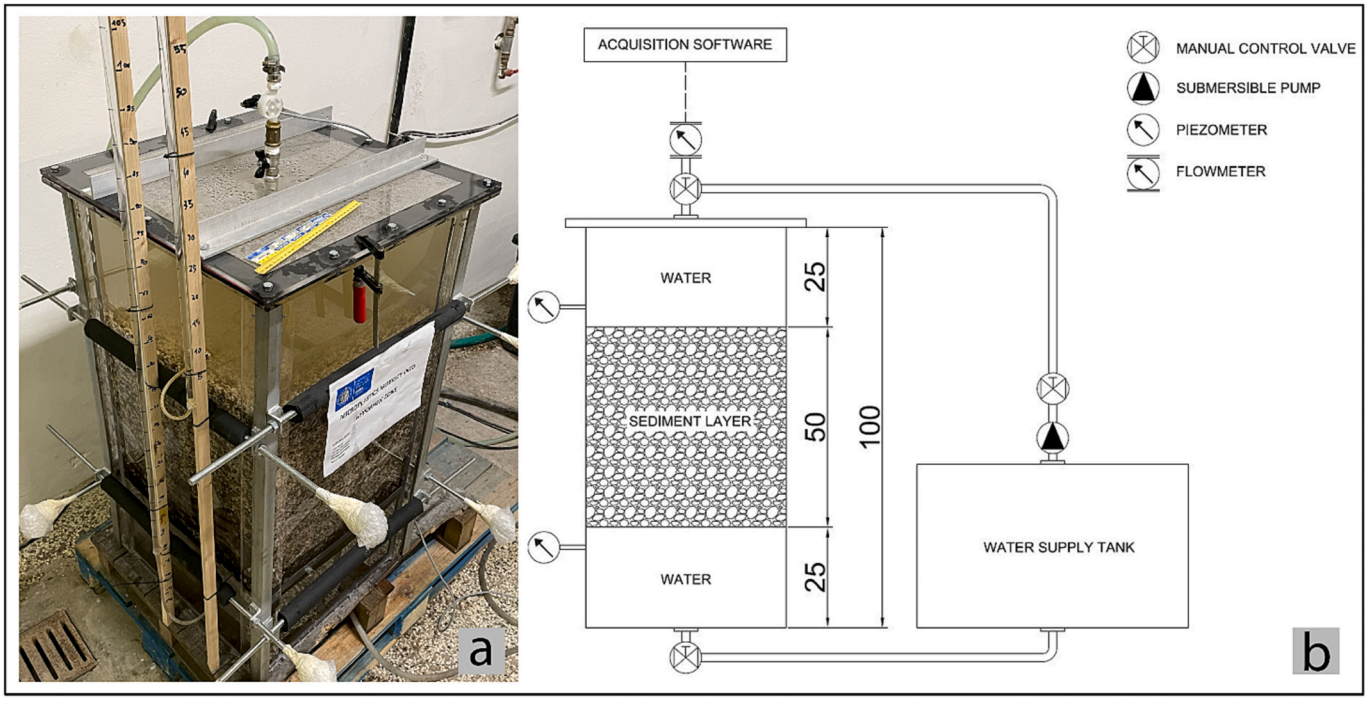

Fig. 2. The plexiglass tank during one of the pressurized tests (a) and a diagram of the experimental setup (b). All measurements are in cm.

Table 1
Experimental conditions considered for each run: Experiment duration (t in h), hydraulic load (H_L in m). Flow rate (Q in m^3/s) was acquired for the entire duration of each experiment using a flowmeter (FCH-midi-POM ®RIELS coupled with the 24 V NI9422 acquisition board and acquisition data software ®LabVIEW 2015) with an acquisition frequency of 1 Hz. The hydraulic conductivity (K in m/s) and the hydraulic gradient (i, dimensionless) were calculated as reported in the theory section. Experiments N° 5 and N° 12 were repeated 3 times to test for replicability.

Run #	Duration – t [h]	Hydraulic load - H_L [m]	Flow rate – Q [m^3/s]	Hydraulic conductivity – K [m/s]	Vertical hydraulic gradient – i [−]	N° of MPs [−]	Sediment type [−]
1	1	0.25	6.6E−5	9E−3	3E−02	180	Fine Gravel - FG
2	5	0.25	6.6E−5	9E−3	3E−02	180	Fine Gravel - FG
3	1	0.65	4.8E−5	1.9E−2	1E−02	180	Fine Gravel - FG
4	5	0.65	4.9E−5	1.6E−2	1.2E−02	180	Fine Gravel - FG
5.1	1	0.25	3.8E−5	1.5E−2	1E−02	180	Medium Gravel -MG
5.2	1	0.25	3.5E−5	1.8E−2	8E−03	180	Medium Gravel -MG
5.3	1	0.25	4E−5	2.7E−2	6E−03	180	Medium Gravel - MG
6	5	0.25	3.8E−5	2.5E−2	6E−03	180	Medium Gravel - MG
7	1	0.65	4.6E−5	4.6E−2	4E−03	180	Medium Gravel - MG
8	5	0.65	4.2E−5	2.8E−2	6E−03	180	Medium Gravel - MG
9	1	0.25	2.5E−5	1.7E−2	6E−03	180	Coarse Gravel - CG
10	5	0.25	3E−5	3E−2	4E−03	180	Coarse Gravel - CG
11	1	0.65	4.5E−5	1E−2	1.8E−02	180	Coarse Gravel - CG
12.1	5	0.65	4.8E−5	1.9E−2	1E−02	180	Coarse Gravel - CG
12.2	5	0.65	4.5E−5	1E−2	1.8E−02	180	Coarse Gravel - CG
12.3	5	0.65	4.0E−5	2E−2	8E−03	180	Coarse Gravel - CG
13	1	0.8	5.3E−5	3.5E−2	6E−03	180	Coarse Gravel - CG
14	5	0.8	5.9E−5	3.9E−2	6E−03	180	Coarse Gravel - CG
15	1	1	5E−5	3.3E−2	6E−03	180	Coarse Gravel - CG
16	5	1	5E−5	2.5E−2	8E−03	180	Coarse Gravel - CG

and the linear regression analysis were performed using OriginPro version 9.0 (OriginLab Corp., US). The Kruskal-Wallis ANOVA tests were also performed with OriginPro version 9.0 to verify the repeatability of the experiments. For all statistical analyses, the significance level applied was $\alpha = 0.05$.

3. Results

3.1. General observations about MP infiltration

At the end of the experimental work, the total number of particles tested was 3300 with a relative error of 0.2 % due to particles lost during some of the experimental sessions. The Kruskal-Wallis ANOVA test

verified the repeatability of the experiments (min *Chi-square* > 0.05, see Tables S3 and S4).

Based on the experiments, some general observations about the infiltration behavior of plastic particles were made. MP that infiltrated deepest were found in the CG sediment layer between 20 and 25 cm. Spheres tend to infiltrate more easily than other particle shapes. No particle reached an infiltration depth (I_{DEPTH}) >10 cm when FG and MG sediments were used, and I_{DEPTH} >10 cm was reached only by the spheres and fragments (Fig. 3). MPs with equal density reached different maximum depths (I_{DEPTH_MAX}); density, therefore, does not seem to influence the MP penetration capacity into saturated sediment layers. On the contrary, the results suggest a slight tendency of the MPs to reach greater infiltration depths for 2D and 3D particles, except for 3D pellets, due to their mean size being comparable to or greater than the sediment cavities' diameter, which makes it difficult to infiltrate and which will be discussed more in-depth further on. However, a quantitative analysis was beyond the main goal of the present work due to the impossibility of separating the influence of the particles' shapes and densities (Fig. 3).

3.2. The influence of time test and hydraulic load

Within the tested t range, t was found to have a low influence on I_{DEPTH_MAX}. Keeping constant the variety of MP types, H_L, and the type of sediment, an increase in test time (t) led to an increase in I_{DEPTH_MAX} only in 20 % of cases: $H_L = 0.25$ m/CG for all MP types, $H_L = 0.65$ m/MG and $H_L = 0.65$ m/CG for PET spheres and $H_L = 0.25$ m/FG for PET 3D-pellets and PET spheres. Moreover, the negligible influence of t may also depend on the maximum H_L value used during the experiments.

A linear regression analysis (Table S5) was performed for the CG case, considering experiments with both $t = 1$ h and $t = 5$ h for each MP type to investigate the influence of H_L on the I_{DEPTH_MAX}. Linear fits of different H_L against I_{DEPTH_MAX} for each run revealed negligible trends with R^2 values ranging between 0.04 and 0.15, except for 0.26 mm-diameter PA fibers, for which the R^2 resulted equal to 0.61. This finding indicates that the effect of the increase in H_L on I_{DEPTH_MAX} seems to be negligible for most MP types and over the H_L range tested.

As stated above, the increased hydraulic load does not seem to affect the maximum infiltration depths; however, it plays a role in increasing the percentage of MPs that penetrate below the superficial layer. Considering the CG sediment size as a reference, results of both 1 h and 5 h test times showed that the average percentage of MPs able to infiltrate below the superficial layer slightly increased with a power trend ($R^2 = 0.89$, p-value = 0.0002) from 52.7 % ($H_L = 0.25$ m) to 61.3 % ($H_L = 1$ m). Particularly, with increasing H_L values, MPs tended to accumulate in the 0–5 cm sediment layer, independently of their type (Fig. 4 and in similar plots in Fig. S1).

3.3. The influence of the sediment and microplastic sizes

The number of MPs within the sediment layer decreased with different power trends as the infiltration depth increased for each type of soil considered and for each combination of H_L and t (Fig. 5 and in similar plots in Fig. S2). Moreover, the I_{DEPTH_MAX} was affected by the sediment size when the MP shape exhibited high roundness (CSF > 0.7). On the contrary, comparable values of the I_{DEPTH_MAX} were found for 1D and 2D shapes (0.11 < CSF < 0.15) (Fig. 5 and in similar plots in Fig. S2). Particularly, for both combinations analyzed ($t = 5$ h/$H_L = 0.25$ m, $t = 5$ h/$H_L = 0.65$ m), findings showed that I_{DEPTH_MAX} increased with increasing the sediment size, mainly for PET spheres and PET 3D-pellets, being higher in panel 4c than 4a and 4b (Fig. 5, and in similar plots in Fig. S2). Again, similarly to what has been observed under the effect of different H_L values, even increasing the D_{50} of the sediment layer, MPs

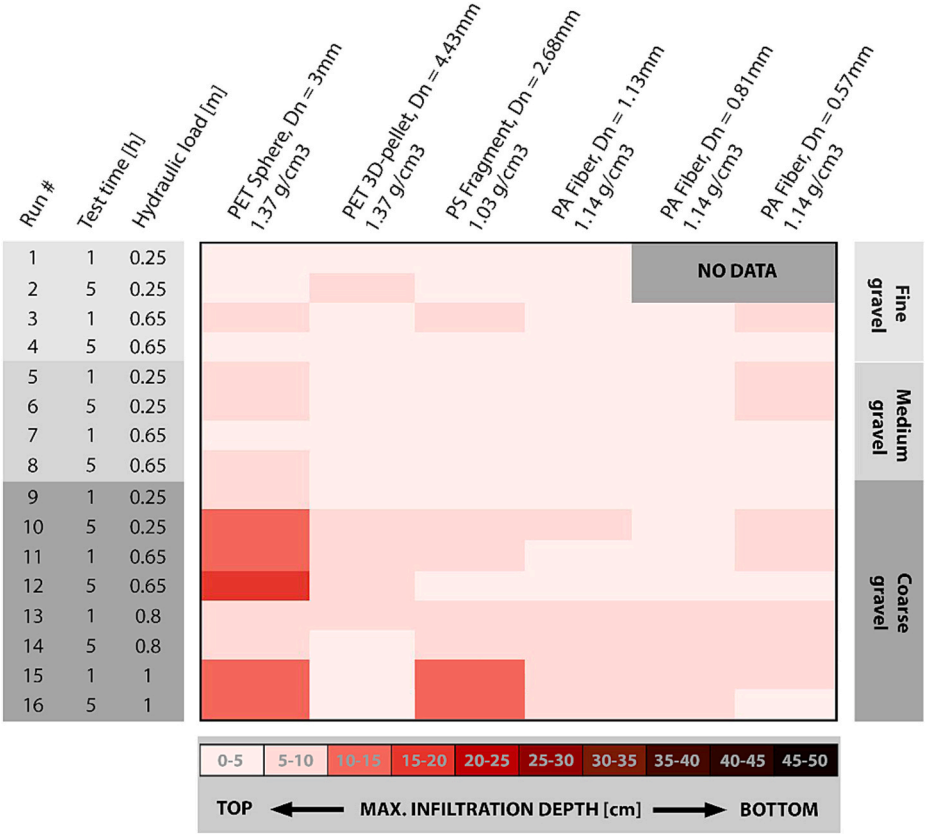

Fig. 3. Heat map of the maximum infiltration depth (I_{DEPTH_MAX}) reached by each type of MP for all the experiments ordered for increasing H_L. Each range of shaded red corresponds to the deepest layer (5 cm thick), where at least 10 % of particles were found. In the experiment's Runs 5 and 12, I_{DEPTH_MAX} was obtained by averaging the maximum depths for all repetitions. D_n represents the equivalent spherical diameter of each type of MP.

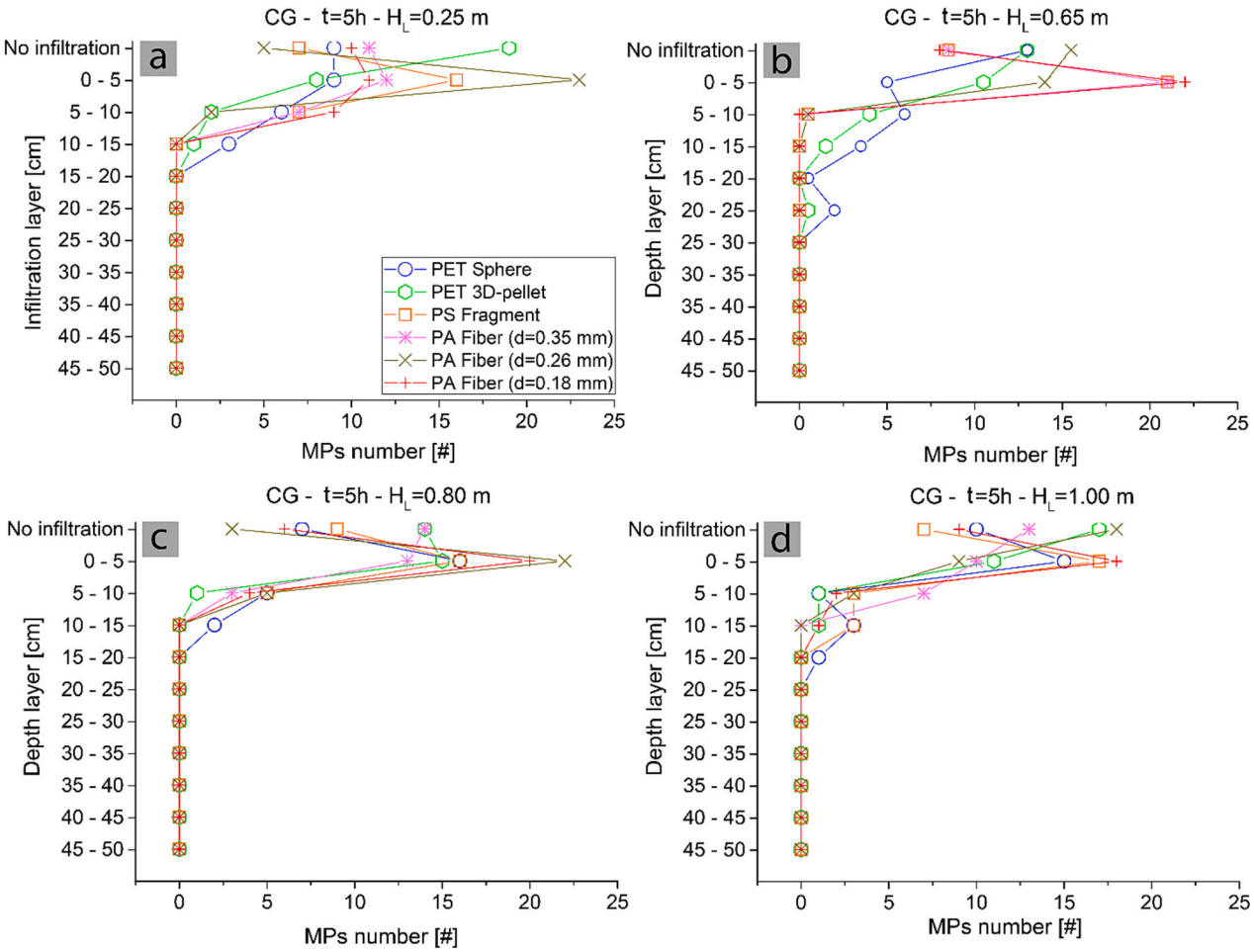

Fig. 4. The number of different types of MPs counted in each infiltration layer (each layer analyzed had a thickness of 5 cm) by using: (a) $H_L = 0.25$ m, (b) $H_L = 0.65$ m, (c) $H_L = 0.8$ m and (d) $H_L = 1$ m with a 5-h duration (t) of the experiment and CG as sediment layer. The term "*No infiltration*" was related to those MPs that, at the end of the experiment, were found in the same position in which they were placed at the beginning. For each experiment, a total of 180 MPs (30 for each type) were used.

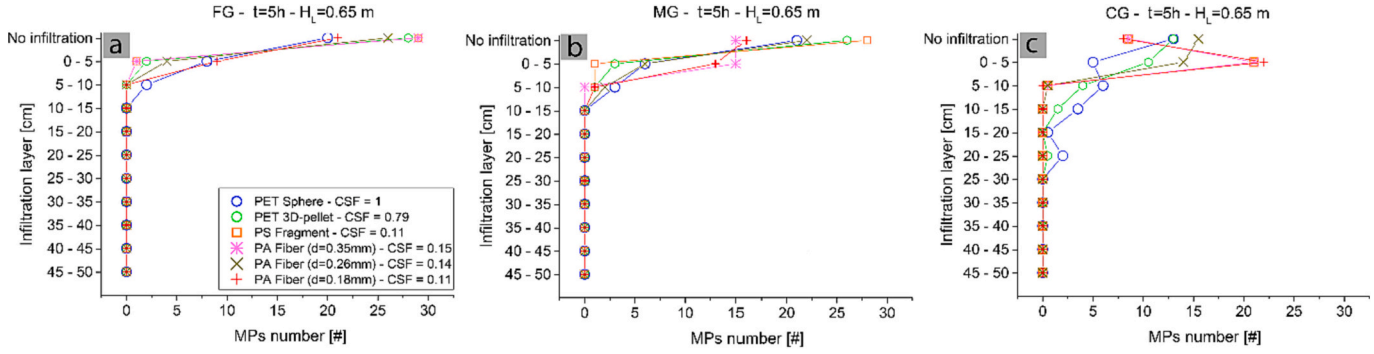

Fig. 5. The number of different types of MPs counted in each infiltration layer (each layer analyzed had a thickness of 5 cm) by using: (a) fine gravel (FG), (b) medium gravel (MG) and coarse gravel (CG) as sediment layer and with a 5-h duration (t) of the experiment and a hydraulic load (H_L) equal to 0.65 m. The term "*No infiltration*" was related to those MPs that were found above the surface at the end of the experiment. For each experiment, a total of 180 MPs (30 for each type) were used.

less likely to infiltrate deeply tended to accumulate in the 0–5 cm sediment layer.

The results of the experiments with $H_L = 0.65$ m in both $t = 1$ h and t = 5 h cases (due to the non-influence of the t variable) also showed that for each type of MPs considered, the percentage of MPs not likely to infiltrate below the superficial layer decreases as the D_{50} increases, resulting in lower than 50 % when the sediment layer D_{50} was set to 15.4 mm (average MP percentages at surface for $D_{50} = 5.05$ mm, 9.45 mm and 15.4 mm equal to 86 ± 8.3 %, 65 ± 16.2 % and 40 ± 12.3 %, respectively). Based on the above findings, the percentage of MPs not able to infiltrate below the superficial layer was investigated in relation to the ratio between the MP maximum diameter (considered the characteristic one for the initial filtration as explained in the theoretical assumption paragraph) and the representative size of sediments (d_{MAX}/

D_{50}) (Fig. 6). The values of d_{MAX}/D_{50} found in this work ranged between 0.19 and 2.75. Thus, once defined 3 intervals of d_{MAX}/D_{50}, we observed that the mean percentage of MPs remaining on the superficial layer ($MP_{SURFACE}$) at the end of each run increased as the ratio itself increased ($MP_{SURFACE} = 54 \pm 19$ % for $d_{MAX}/D_{50} < 0.5$, $MP_{SURFACE} = 61 \pm 23$ % for $0.5 < d_{MAX}/D_{50} < 1$, $MP_{SURFACE} = 73 \pm 19$ % for $d_{MAX}/D_{50} > 1$). Moreover, the $MP_{SURFACE}$ increased as the MP d_{MAX} increased. By averaging the $MP_{SURFACE}$ among all the types of soils, we obtained $MP_{SURFACE} = 60$ % for $d_{MAX} \approx 13$ mm (PA fibers), $MP_{SURFACE} = 63.3$ % for $d_{MAX} = 5.4$ mm (PS fragments) and $MP_{SURFACE} = 66$–72 % for $d_{MAX} = 3$–4.2 mm (PET 3D-pellets, PET spheres) (Fig. 6).

As a first approach, we studied deep infiltration, assuming that MPs move within the sediment layer following the same arrangement they have in the case of initial filtration. Thus, results can be expressed in dimensionless form by introducing the ratio of the two characteristic length scales of the process, which are the infiltration depth (I_{DEPTH}) and the maximum diameter of MP particles (d_{MAX}). Considering the CG sediment layer, the relative number of MPs collected above each layer depth is expressed as a function of the ratio I_{DEPTH}/d_{MAX} for different values of H_L and the six groups of particles (Fig. 7): PET spheres (CSF = 1), as already shown in Figs. 4 and 5, infiltrated more than the other MP types for all the H_L tested, followed by PET 3D-pellets (CSF = 0.79), PA fibers (d = 0.35 mm, CSF = 0.15), PA fibers (d = 0.26 mm, CSF = 0.14), PS fragments (CSF = 0.11) and PA fibers (d = 0.18 mm, CSF = 0.11), showing that the I_{DEPTH} was strongly related to the CSF, with direct proportionality. Again, by relating the relative number of MPs collected above each layer depth with I_{DEPTH}/d_{MAX}, we extrapolated the best fit, limited to PET spheres and PET 3D-pellets (in the cases of CG, $H_L = 0.25$ m, 0.65 m, 0.8 m and 1 m) (Fig. 8), which showed how the two types of particles infiltrated into sediments with different power trends ($Y = 0.414 \bullet X^{0.211}$ and $Y = 0.787 \bullet X^{0.065}$ for PET spheres and PET 3D-pellets, respectively) with I_{DEPTH}/d_{MAX} values ranging in between 0 and 83.3 for PET spheres and between 0 and 58.3 for PET 3D-pellets. For the other types of particles, a fit was deemed non-significant, given the low number of data points available.

According to the theoretical assumptions about deep infiltration, the effect of the minimum MP diameter (d_{MIN}) in affecting the I_{DEPTH_MAX} of the MPs was also investigated. The dimensionless graph shown in Fig. 9 gives experimental data (for all experimental runs) plotted in terms of force ratio F_D/F_I vs I_{DEPTH_MAX}/d_{MIN} ratio. I_{DEPTH_MAX}/d_{MIN} increased as F_D/F_I increased with a power trend $Y = 1.46 \cdot X^{0.35}$ ($R^2 = 0.67$, p-value = 1.77E−15). Also, MPs with very high CSF (>0.75) presented a relative I_{DEPTH_MAX} smaller than those with low CSF (≈0.1), except for PS fragments for which the infiltration capacity appeared similar to those MPs with a slightly larger CSF. However, I_{DEPTH_MAX}/d_{MIN} of MP with very high CSF (0.8–1) seemed to be hardly affected by the F_D/F_I, showing an approximately constant value equal to $I_{DEPTH\_MAX}/d_{MIN} = 27.8 \pm 11.7$. On the contrary, when we moved to the MPs with low CSF (≈0.1), I_{DEPTH_MAX}/d_{MIN} exhibited a high correlation with the F_D/F_I ratio, rapidly decreasing from $I_{DEPTH\_MAX}/d_{MIN} = 555.5$ to 100 as F_D/F_I decreased. This result may suggest that there is some threshold mechanics in F_D/F_I below which particle mobility is greatly enhanced. As a consequence, they infiltrate better in the sediment layer.

4. Discussion

4.1. The implication in MP retention into superficial sediment layer

The current work provided information on the main parameters driving the MP infiltration within the gravel sediment layer under different hydraulic conditions, confirming the ratio between the MP characteristic diameter and the D_{50} of the soil as one of the fundamental parameters for evaluating the initiation of infiltration. The lower the d_{MAX}/D_{50}, the greater the MP percentage likely to penetrate the superficial sediment layer (Fig. 6). Thus, for $d_{MAX}/D_{50} > 1$ values, high MP rates (> 90 %) might be forced to remain on top of the riverbed, becoming easily transportable by the flow at a great distance from their source.

In rivers, sediment size decreases exponentially from headwater to downstream due to riverbed abrasion processes (Sternberg, 1875) and size-selecting sorting (Paola et al., 1992). Accordingly, the findings above suggest that MPs may be less inclined to be transported in the rivers' upper part than downstream.

MPs that were able to infiltrate are suspected to likely accumulate and be stored for a long time in the riverbed sediment layer (Drummond et al., 2022) and potentially contaminate groundwater (Chia et al., 2021). However, the results from the present study demonstrated that most of the MPs with d_{MIN} ranging between 3 mm and 0.18 mm were retained within the first 15 cm of soil in the case of sediment layers characterized by a D_{50} ranging from about 5 mm to 15 mm. In contrast, an increase in H_L did not change I_{DEPTH_MAX}. Instead, H_L affected the number of MPs that could infiltrate and their distribution within the 0–15 cm sediment layer.

The results above seem to confirm what was found by McDowell-Boyer et al. (1986) about particles transported through porous media, which provided a threshold value for the change in the transport mechanism based on the ratio between the diameter of the suspended particles (d_p) and that of the grains composing the porous medium (d_g).

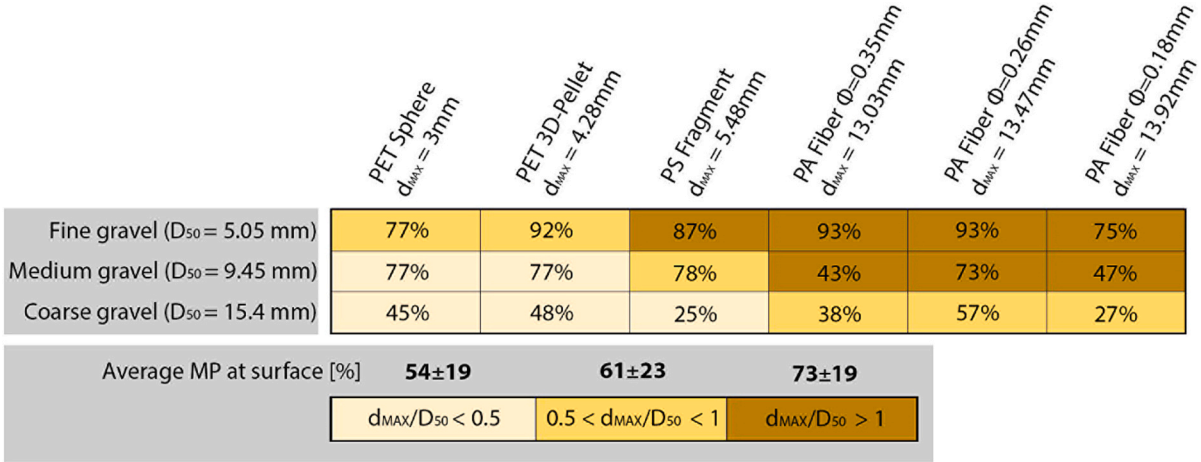

Fig. 6. Percentage of different types of MPs which did not infiltrate at the end of each run by varying sizes of gravel forming the sediment layer. Also, the mean percentage of the non-infiltrated MPs in combination with different d_{MAX}/D_{50} ratios was given. The calculations refer to the following conditions: $H_L = 0.65$ m and $t = 1$ and 5 h.

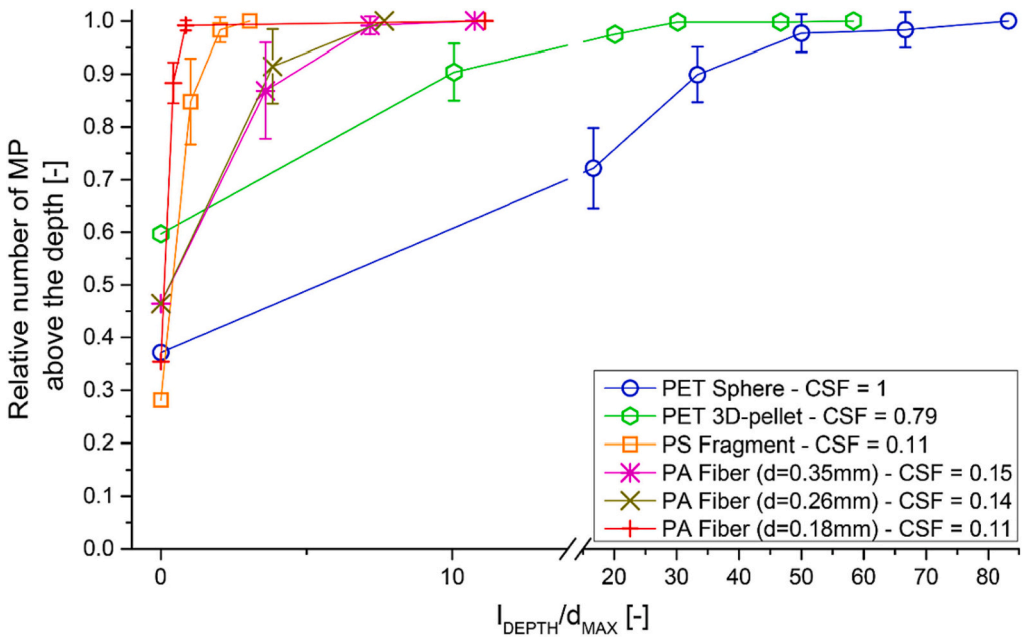

Fig. 7. Relative cumulative distribution for each group of tested MPs versus the I_{DEPTH}/d_{MAX} ratio, in the case of CG sediment layer. Error bars were calculated using the standard deviation between the values obtained for different H_L. (The horizontal axis has two scales for readability purposes).

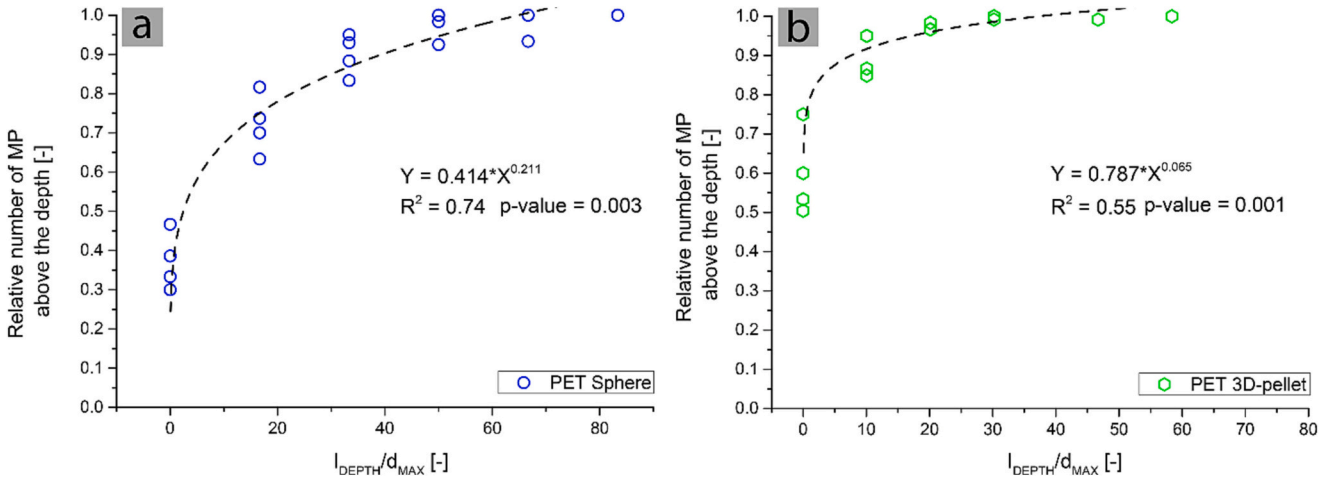

Fig. 8. Relative cumulative distribution of PET spheres (a) and PET 3D-pellets (b) versus the I_{DEPTH}/d_{MAX} ratio, considering all the hydraulic load ($H_L = 0.25$ m, 0.65 m, 0.8 m and 1 m) and the CG sediment layer.

The authors recognized the ratio $d_p/d_g \geq 0.1$ as the threshold above which the straining is the predominant mechanism in retaining particles. The latter leads to hypothesize that, under low and medium water level conditions (up to 1 m as far as our study is concerned), MPs previously stored in sediment may tend to remain buried just below the surface even for long periods of time due to mechanical blockage. Instead, most MPs may be already resuspended by floods remobilizing only the most superficial layers of the riverbed. Still, MPs stored in superficial layers are more subject to mechanical wearing and chemical degradation processes like solar irradiation (Alimi et al., 2018) than those buried deep down in the soil. Therefore, such conditions could favor their fragmentation into smaller MPs or nano plastic particles more likely to infiltrate at greater depths, affecting the process of groundwater contamination. Consequently, different grain sizes of the riverbed sediment could help sorting MP sizes transported downstream. The different granulometric distribution of the riverbed should therefore be taken into consideration in developing further MP transport models in freshwater environments.

4.2. Physical interpretation of the model

This work showed that the initial filtration of MP can be well described using d_{MAX} as a characteristic diameter. Results seem to suggest that during the initial filtration, the percentage of PA fibers likely to infiltrate just below the superficial layer was greater than that of the other MP type; however, PA fibers were found unable to penetrate further than 10 cm deep. Additionally, the model given in Fig. 9 for deep infiltration suggested that the bigger the MP mobility, the bigger the CSF of the particles, exhibiting threshold mechanics for a certain F_D/F_I value. A physical interpretation of the abovementioned should lead to the conclusion that the more elongated the particles (low CSF), the more they are subject to bending along the minor axis (d_{MIN}). Thus, for fibers, the initial filtration could be facilitated by the fact that they can easily bend, significantly reducing their d_{MAX} below that of the other MP types.

Similarly, under deep filtration conditions, fibers initially aligned with the flow (d_{MIN} orientated perpendicular to the settling direction) will begin a tumbling motion caused by relatively high shear stress

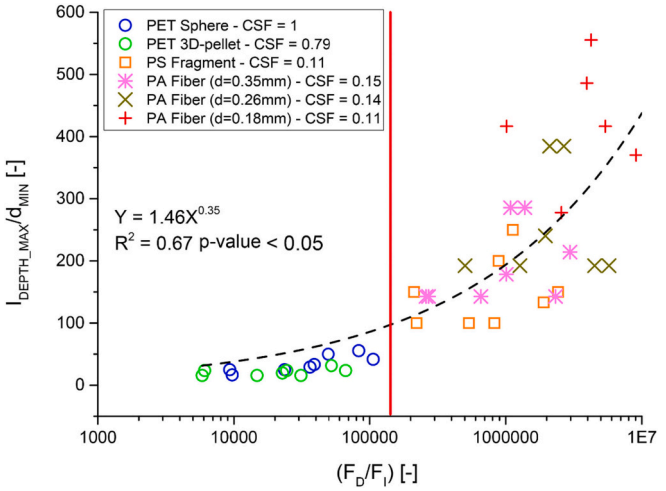

Fig. 9. Relationship between F_D/F_I and I_{DEPTH_MAX}/d_{MIN} for all the experiments carried out. The red line represents the transition between the two trends observed from the data.

produced by the flow and this process will increase in proximity to the walls as already found by Słowicka et al. (2012). Thus, in our case, for values of F_D/F_I above a certain threshold, fibers no longer aligned with the flow might be more prone to be trapped by grain protrusions, making it difficult for them to infiltrate deeper. However, more experiments ought to be carried out along these lines, using the same particle volume and density but different shapes, to better determine the effect of the shape itself on the I_{DEPTH_MAX}.

The model presented in this study describes MPs infiltration within saturated natural sediment layers, however it cannot directly incorporate all the complex processes that take place within the hyporheic zone. First, the model does not consider possible effects of degradation and fragmentation that could help in increasing the mobility and consequently the I_{DEPTH_MAX} of MPs within the sediment layer. Also, biological factors could influence MP mobility: as observed by Näkki et al. (2017) bioturbation might enhance the MP transport to the deepest layer of sediments while biofouling may decrease it by increasing the MP size. Finally, additional hydrodynamic factors like turbulence, hydropeaking and horizontal flows could affect time scales of MP infiltration processes, thus resulting of interest for further investigations.

4.3. Comparison with previous experimental findings

The results of this work were compared to recent studies investigating the infiltration behavior of several types of MPs within porous sediment layers from different standpoints (Table 2). Firstly, given the similarity of the setup, we compared our outcomes with what was found by Waldschläger and Schüttrumpf (2020). To investigate the reliability of the comparison, we checked the similarity of the flow values through the pores (Q), the sediment sizes (D_{50}) (glass spheres in the case of Waldschläger and Schüttrumpf, 2020), the MP types (in shape, size, and density) and the test time (T) used in the two works. Results are summarized in Table 2 below.

The results of the comparison are reported in Fig. 10, showing a discrepancy in the respective trends for $D_{50} > 0.005$ m. In the present study, the MP particles tended to infiltrate less than Waldschläger and Schüttrumpf (2020) found. This discrepancy could be attributed to the use of glass spheres by the latter instead of natural sediments to simulate the sediment layer. As suggested by Rodrigues et al. (2023), the tortuosity (τ), defined as the ratio of the increased tortuous path length to the thickness of the porous medium, decreases as the sphericity (ϕ) of the particles in the porous medium increases. Thus, since natural sediments clearly have lower sphericity than manufactured glass spheres, the

Table 2
Specific parameters considered in the comparison between the present study and similar works. In order to compare the size of MP, d_{MP} was calculated as reported in Waldschläger and Schüttrumpf (2020). For fragments investigated by Wang et al. (2021a), the d_{sieve} (the MP diameter obtained by screening particles using sieves with different mesh sizes) was used instead, due to the missing data necessary to calculate the d_{MP}. In the present study, both $t = 1$ h and $t = 5$ h are taken into account because they didn't show any correlation with the I_{DEPTH_MAX} (see Results section).

	Waldschläger and Schüttrumpf (2020)	Wang et al. (2021a)	Present study
MP type (Shape, size, and type of material)	PET, PP, PE, PVC and PA spheres (Mean $d_{MP} = 3.45 \pm 1.47$) and pellets (Mean $d_{MP} = 2.97 \pm 0.72$) PET, *Co*-PA, PP and PE fibers (Mean $d_{MP} = 1.53 \pm 0.55$ mm)	PE spheres ($d_{MP} = 0.045$–0.053 mm) PS, HDPE and PP fragments ($d_{sieve} = 0.075$–0.425 mm)	PET spheres ($d_{MP} = 1$ mm), PET 3D-pellets ($d_{MP} = 3.41$ mm) PA fibers (Mean $d_{MP} = 0.97 \pm 0.21$ mm)
Q [m^3/s]	$7.66*10^{-5}$	Missing	$4.6*10^{-5} \pm 1.08*10^{-5}$
Particle size making up the sediment layer [mm]	$D_{50} = 6$; 8 and 11 (glass spheres)	0.356 (sand) $2 < 30\ \% < 5.6$ $5.6 < 70\ \% < 8$	$D_{50} = 5.05$; 9.45 and 15.4
t [h]	1	120–1080	1;5

greater value of τ can be attributed to the sediment layer used in this work, which could cause the reduced MP infiltration capacity, assuming consistency of all other parameters. Additionally, the MP I_{DEPTH_MAX} for small natural sediments was close to that of spherical glass particles. This might be caused by the fact that the smaller the natural sediments, the more spherical their shape (Domokos et al., 2014). In contrast, I_{DEPTH_MAX} for large natural sediment particles shifted from that of large glass spheres. Finally, the greater roughness of natural sediments, compared to smooth glass surfaces, could further affect the MP's ability to be carried by the flow inside the porous cavities. However, this work did not investigate microscopic scale effects like the one mentioned above, and more in-depth studies are needed.

The above statements suggest that further investigations about MP infiltration in porous media need to be coupled with a detailed characterization of the porous medium itself, mainly in terms of sediment size and shape, to better comprehend how MPs are distributed inside.

The results of this work can also be regarded as informative additional data on the use of sediment filters to reduce MP pollution by wastewater treatment plants. Using this standpoint, a reasonable comparison should be made with the findings of Wang et al. (2021a) (Table 2), in which the MP retention capacity of sand- and gravel-filled vertical flow constructed wetlands was investigated. Ignoring the experiments where biofilm and heartworms were added to the sediment layer, we compared the I_{DEPTH_MAX} found by Wang et al. (2021a) with those observed in our work, considering the ratio (R) between the MP diameter (d_{MP} for this study and d_{sieve} for Wang et al.'s (2021a)) and the D_{50}. The comparison revealed a substantial alignment of data. When the ratio R was similar between the two works ($d_{MP}/D_{50} = 1.48$–4.5 and $d_{sieve}/D_{50} = 0.21$–1.19), the I_{DEPTH_MAX} was found in the range between 5 and 15 cm depending on the particle type; when the ratio R was higher, between 0.0093 and 0.21, greater I_{DEPTH_MAX} were found in Wang et al. (2021a). However, this might be explained by considering the effect of the MPs with different CSF used in this last comparison (fragments for Wang et al. (2021a) and fibers for the present study).

Moreover, when the ratio R was in the range 0.0093–0.21, we observed a similar distribution in the MP concentration along the depth, exhibiting its maximum in the layers immediately below the superficial

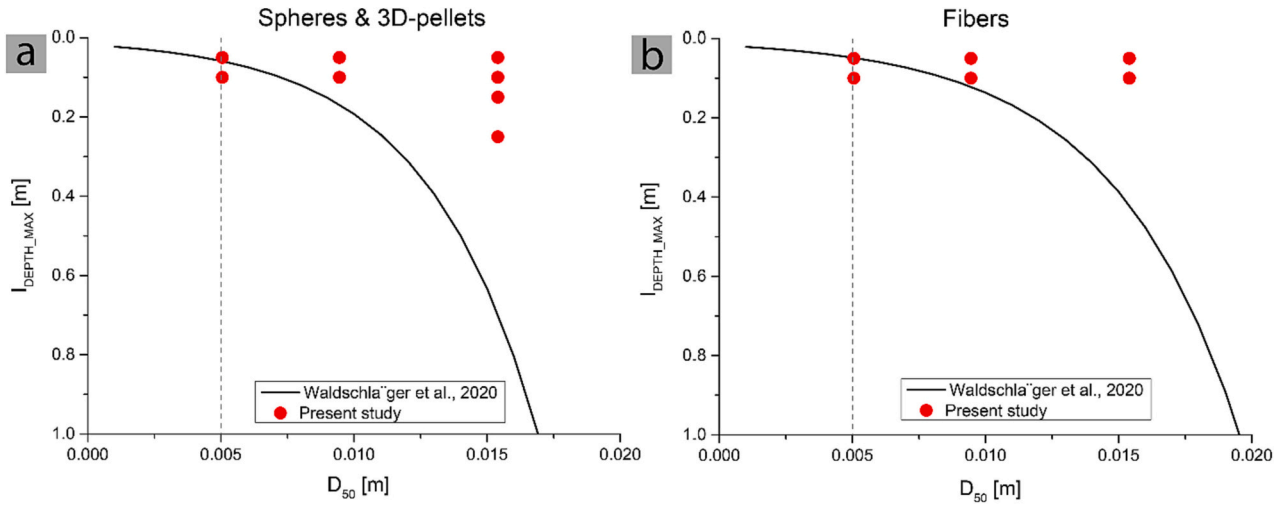

Fig. 10. I_{DEPTH_MAX} measured in the present study for PET spheres and PET 3D-pellets under conditions given in Table 2. The solid lines are equations given by Waldschläger and Schüttrumpf (2020), valid for spheres and pellets (a) and for fibers (b) by assuming the conditions summarized in Table 2. The dashed lines represent the limit of D_{50} above which the data points of the present study begin to diverge from the equations given by Waldschläger and Schüttrumpf (2020).

one (5–10 cm) in both studies. Unfortunately, data about the Q are missing (only a constant H_L = 0.08 m is given). The time t of each experimental session ranged from 120 h to 1080 h (orders of magnitude greater than those used in the present study), and mostly, it was not possible to give the size of MPs in terms of the d_{MP} instead of the d_{sieve}; thus a very detailed comparison was not feasible (Table 2). However, the fact that we obtained similar results for different H_L and t values seemed to confirm the negligible role of these two parameters in affecting the I_{DEPTH_MAX}, as previously pointed out in our experiments.

5. Conclusions

This study investigates the effects of hydraulic load (H_L), time duration (t) as well as MP physical properties (shape, size, and type of polymer) and the grain size of the sediment layer (D_{50}) on the infiltration capacity and retention of four different types of MPs in saturated porous media. A model able to predict the maximum penetration depth (I_{DEPTH_MAX}) was presented as a function of both the characteristics of the sediment layer and the MPs. Regardless of the conditions, none of the plastic particles (0.5–5 mm) could infiltrate >20–25 cm deep. Thus, this work highlights the high MP retention capacity of natural gravel layers and their suitability to be used as filters to mitigate MP pollution. The increase of the H_L and t do not correspond to an increase in the maximum MP penetration depth (I_{DEPTH_MAX}). However, the number of MPs penetrating the surface layer of sediment increases as the H_L increases. Nevertheless, the relationship d_{MAX}/D_{50} was found to be the main parameter driving the MPs' infiltration capacity. Results also suggested the role of the CSF in affecting MPs' deep infiltration with greater I_{DEPTH_MAX} when CSF has higher values; moreover, experimental observations suggested the existence of an MP mobility threshold when the force ratio F_D/F_I was less than a certain threshold.

The results of this work and the implications discussed above point out the fundamental role played by different types of riverbed sediments in avoiding or promoting the MP storage in riverbeds, also highlighting the importance of the need to characterize the riverbed granulometry to predict the actual MP load discharged to the sea. Further laboratory experiments should extend the investigation to other types of MPs (e.g. floating MPs), of smaller size, and to test a wider range of hydraulic loads (HL) and time durations (t). Hydrodynamics of the hyporheic zone is very complex and characterized not only by unidirectional water flows from the superficial sediment layers to the groundwater, thus additional effects like water exchange with streams, horizontal flow, turbulence, hydropeaking, thermal peaking should be considered in the future.

Funding

This study was supported by research program "PE3 – Rischi ambientali, naturali e antropici – RETURN – Multi-risk science for resilient communities under changing climate" as part of the National Recovery and Resilience Plan – NextGenerationEU – CUP B83C22004820002 and by Pegaso Scholarships funded by the Regione Toscana. The authors also received partial funding within the project "Plastics balance in the Arno River-Coastal basin and analysis of recovery and recycling technologies in civil and environmental works" (Fondazione CR Firenze, 2021).

CRediT authorship contribution statement

Mirco Mancini: Conceptualization, Methodology, Software, Formal analysis, Investigation, Writing – original draft, Writing – review & editing, Visualization. **Simona Francalanci:** Conceptualization, Methodology, Validation, Resources, Writing – original draft, Writing – review & editing, Supervision. **Lorenzo Innocenti:** Conceptualization, Methodology, Validation, Writing – original draft, Writing – review & editing, Visualization, Supervision. **Luca Solari:** Conceptualization, Methodology, Validation, Resources, Writing – original draft, Writing – review & editing, Supervision.

Declaration of competing interest

The authors declare that they have no known competing financial interests or personal relationships that could have appeared to influence the work reported in this paper.

Data availability

Data will be made available on request.

Acknowledgements

We are grateful to the Laboratory of Fluvial Hydraulics, Lagoon and Biofluidodynamics of the Department of Civil and Environmental Engineering - University of Florence for all the technical assistance provided to develop this project. We would also like to thank Eng. Muzio Mascherini for all the technical help provided.

Appendix A. Supplementary data

Supplementary data to this article can be found online at https://doi.org/10.1016/j.scitotenv.2023.167256.

References

Albar, A., 2000. Effect of Various Terminal Velocity Equations on the Result of Friction Loss Calculation, 13.

Alimi, O.S., Farner Budarz, J., Hernandez, L.M., Tufenkji, N., 2018. Microplastics and nanoplastics in aquatic environments: aggregation, deposition, and enhanced contaminant transport. Environ. Sci. Technol. 52 (4), 1704–1724. American Chemical Society. https://doi.org/10.1021/acs.est.7b05559.

Becucci, M., Mancini, M., Campo, R., Paris, E., 2022. Microplastics in the Florence wastewater treatment plant studied by a continuous sampling method and Raman spectroscopy: a preliminary investigation. Sci. Total Environ. 808, 152025. https://doi.org/10.1016/j.scitotenv.2021.152025.

Boano, F., Harvey, J.W., Marion, A., Packman, A.I., Revelli, R., Ridolfi, L., Wörman, A., 2014. Hyporheic flow and transport processes: mechanisms, models, and biogeochemical implications. Rev. Geophys. 52 (4), 603–679. Blackwell Publishing Ltd. https://doi.org/10.1002/2012RG000417.

Bradney, L., Wijesekara, H., Palansooriya, K.N., Obadamudalige, N., Bolan, N.S., Ok, Y. S., Rinklebe, J., Kim, K.H., Kirkham, M.B., 2019. Particulate plastics as a vector for toxic trace-element uptake by aquatic and terrestrial organisms and human health risk. Environ. Int. 131 https://doi.org/10.1016/j.envint.2019.104937. Elsevier Ltd.

Chia, R.W., Lee, J.Y., Kim, H., Jang, J., 2021. Microplastic pollution in soil and groundwater: a review. Environ. Chem. Lett. 19 (6), 4211–4224. Springer Science and Business Media Deutschland GmbH. https://doi.org/10.1007/s10311-021-01297-6.

Colomer, J., Müller, M.F., Barcelona, A., Serra, T., 2019. Mediated food and hydrodynamics on the ingestion of microplastics by *Daphnia magna*. Environ. Pollut. 251, 434–441. https://doi.org/10.1016/j.envpol.2019.05.034.

Dhivert, E., Phuong, N.N., Mourier, B., Grosbois, C., Gasperi, J., 2022. Microplastic trapping in dam reservoirs driven by complex hydrosedimentary processes (Villerest Reservoir, Loire River, France). Water Res. 225 https://doi.org/10.1016/j.watres.2022.119187.

Domokos, G., Jerolmack, D.J., Sipos, A.Á., Török, Á., 2014. How river rocks round: resolving the shape-size paradox. PLoS One 9 (2). https://doi.org/10.1371/journal.pone.0088657.

Drummond, J.D., Nel, H.A., Packman, A.I., Krause, S., 2020. Significance of hyporheic exchange for predicting microplastic fate in rivers. Environ. Sci. Technol. Lett. 7 (10), 727–732. https://doi.org/10.1021/acs.estlett.0c00595.

Drummond, J.D., Schneidewind, U., Li, A., Hoellein, T.J., Krause, S., Packman, A.I., 2022. Microplastic accumulation in riverbed sediment via hyporheic exchange from headwaters to mainstems. Environ. Stud. 8 (2).

van Emmerik, T., Mellink, Y., Hauk, R., Waldschläger, K., Schreyers, L., 2022. Rivers as plastic reservoirs. Front. Water 3. https://doi.org/10.3389/frwa.2021.786936.

Engdahl, N.B., 2018. Simulating the mobility of micro-plastics and other fiber-like objects in saturated porous media using constrained random walks. Adv. Water Resour. 121, 277–284. https://doi.org/10.1016/j.advwatres.2018.08.011.

Folk, R.L., William Ward, X.C., 1957. Brazos River Bar: A Study in the Significance of Grain Size Parameters, 27. Issue 1.

Francalanci, S., Paris, E., Solari, L., 2021. On the prediction of settling velocity for plastic particles of different shapes. Environ. Pollut. 290 https://doi.org/10.1016/j.envpol.2021.118068.

Frei, S., Piehl, S., Gilfedder, B.S., Löder, M.G.J., Krutzke, J., Wilhelm, L., Laforsch, C., 2019. Occurence of microplastics in the hyporheic zone of rivers. Sci. Rep. 9 (1) https://doi.org/10.1038/s41598-019-51741-5.

Gasperi, J., Dris, R., Bonin, T., Rocher, V., Tassin, B., 2014. Assessment of floating plastic debris in surface water along the Seine River. Environ. Pollut. (Barking, Essex: 1987) 195, 163–166. https://doi.org/10.1016/j.envpol.2014.09.001.

Ghinassi, M., Michielotto, A., Ugualgliati, F., Zattin, M., 2023. Mechanisms of microplastics trapping in river sediments: insights from the Arno river (Tuscany, Italy). Sci. Total Environ. 866 https://doi.org/10.1016/j.scitotenv.2022.161273.

Goral, K.D., Guler, H.G., Larsen, B.E., Carstensen, S., Christensen, E.D., Kerpen, N.B., Schlurmann, T., Fuhrman, D.R., 2023. Settling velocity of microplastic particles having regular and irregular shapes. Environ. Res. 228 https://doi.org/10.1016/j.envres.2023.115783.

Hidalgo-Ruz, V., Gutow, L., Thompson, R.C., Thiel, M., 2012. Microplastics in the marine environment: a review of the methods used for identification and quantification. Environ. Sci. Technol. https://doi.org/10.1021/es2031505.

Hurley, R., Woodward, J., Rothwell, J.J., 2018. Microplastic contamination of river beds significantly reduced by catchment-wide flooding. Nat. Geosci. 11 (4), 251–257. https://doi.org/10.1038/s41561-018-0080-1.

Jiang, S., Wang, J., Wu, F., Xu, S., Liu, J., Chen, J., 2023. Extensive abundances and characteristics of microplastic pollution in the karst hyporheic zones of urban rivers. Sci. Total Environ. 857 https://doi.org/10.1016/j.scitotenv.2022.159616.

Khatmullina, L., Isachenko, I., 2017. Settling velocity of microplastic particles of regular shapes. Mar. Pollut. Bull. 114 (2), 871–880. https://doi.org/10.1016/j.marpolbul.2016.11.024.

Khilar, K.C., Fogler, H.S., Gray, D.H., 1985. Model for piping-plugging in earthen structures. J. Geotech. Eng. 111, 833–846.

Kukkola, A., Runkel, R.L., Schneidewind, U., Murphy, S.F., Kelleher, L., Sambrook Smith, G.H., Nel, H.A., Lynch, I., Krause, S., 2023. Prevailing impacts of river management on microplastic transport in contrasting US streams: rethinking global microplastic flux estimations. Water Res. 240, 120112. https://doi.org/10.1016/j.watres.2023.120112.

Kumar, R., Sharma, P., Verma, A., Jha, P.K., Singh, P., Gupta, P.K., Chandra, R., Vara Prasad, P.V., 2021. Effect of physical characteristics and hydrodynamic conditions on transport and deposition of microplastics in riverine ecosystem. Water (Switzerland) 13 (19). https://doi.org/10.3390/w13192710. MDPI.

Lebreton, L.C.M., Van Der Zwet, J., Damsteeg, J.W., Slat, B., Andrady, A., Reisser, J., 2017. River plastic emissions to the world's oceans. Nat. Commun. 8 https://doi.org/10.1038/ncomms15611.

Ling, X., Yan, Z., Lu, G., 2022. Vertical transport and retention behavior of polystyrene nanoplastics in simulated hyporheic zone. Water Res. 219. https://doi.org/10.1016/j.watres.2022.118609.

Magni, S., Binelli, A., Pittura, L., Avio, C.G., Della Torre, C., Parenti, C.C., Gorbi, S., Regoli, F., 2019. The fate of microplastics in an Italian wastewater treatment plant. Sci. Total Environ. 652 https://doi.org/10.1016/j.scitotenv.2018.10.269.

Marot, D., Benamar, A., 2013. Suffusion, transport and filtration of fine particles in granular soil. Eros. Geomater. 39–79. John Wiley and Sons. https://doi.org/10.1002/9781118561737.ch2.

McDowell-Boyer, L.M., Hunt, J.R., Sitar, N., 1986. Particle transport through porous media. Water Resour. Res. 22 (13), 1901–1921. https://doi.org/10.1029/WR022i013p01901.

Meijer, L.J.J., Van Emmerik, T., Van Der Ent, R., Schmidt, C., Lebreton, L., 2021. More than 1000 rivers account for 80% of global riverine plastic emissions into the ocean. Sci. Adv. 7. https://www.science.org.

Morritt, D., Stefanoudis, P.V., Pearce, D., Crimmen, O.A., Clark, P.F., 2014. Plastic in the Thames: a river runs through it. Mar. Pollut. Bull. 78 (1–2), 196–200. https://doi.org/10.1016/j.marpolbul.2013.10.035.

Näkki, P., Setala, O., Lehtiniemi, M., 2017. Bioturbation transports secondary microplastics to deeper layers in soft marine sediments of the northern Baltic Sea. Mar. Pollut. Bull. 119, 255–261. https://doi.org/10.1016/j.marpolbul.2017.03.065.

Paola, C., Parker, G., Seal, R., Sinha, S.K., Southard, J., Wilcock, P.R., 1992. Downstream fining by selective deposition in a laboratory flume. Science 258.

Razeghi, N., Hamidian, A.H., Wu, C., Zhang, Y., Yang, M., 2021. Microplastic sampling techniques in freshwaters and sediments: a review. Environ. Chem. Lett. 19 (6), 4225–4252. Springer Science and Business Media Deutschland GmbH. https://doi.org/10.1007/s10311-021-01227-6.

Reddi, L.N., Lee, I., Bonala, M.V.S., 2000. Comparison of internal and surface erosion using flow pump test on a sand-kaolinite mixture. Geotech. Test. J. 23, 116–122.

Rodrigues, M.O., Abrantes, N., Gonçalves, F.J.M., Nogueira, H., Marques, J.C., Gonçalves, A.M.M., 2018. Spatial and temporal distribution of microplastics in water and sediments of a freshwater system (Antuã River, Portugal). Sci. Total Environ. 633, 1549–1559. https://doi.org/10.1016/j.scitotenv.2018.03.233.

Rodrigues, S.J., Vorhauer-Huget, N., Richter, T., Tsotsas, E., 2023. Influence of particle shape on tortuosity of non-spherical particle packed beds. Processes 11 (1). https://doi.org/10.3390/pr11010003.

Scherer, C., Weber, A., Stock, F., Vurusic, S., Egerci, H., Kochleus, C., Arendt, N., Foeldi, C., Dierkes, G., Wagner, M., Brennholt, N., Reifferscheid, G., 2020. Comparative assessment of microplastics in water and sediment of a large European river. Sci. Total Environ. 738 https://doi.org/10.1016/j.scitotenv.2020.139866.

Scheurer, M., Bigalke, M., 2018. Microplastics in Swiss floodplain soils. Environ. Sci. Technol. 52 (6), 3591–3598. https://doi.org/10.1021/acs.est.7b06003.

Schmidt, C., Krauth, T., Wagner, S., 2017. Export of plastic debris by rivers into the sea. Environ. Sci. Technol. 51 (21), 12246–12253. https://doi.org/10.1021/acs.est.7b02368.

Schwarz, A.E., Ligthart, T.N., Boukris, E., van Harmelen, T., 2019. Sources, transport, and accumulation of different types of plastic litter in aquatic environments: a review study. Mar. Pollut. Bull. 143, 92–100. https://doi.org/10.1016/j.marpolbul.2019.04.029.

Selvam, S., Jesuraja, K., Venkatramanan, S., Roy, P.D., Jeyanthi Kumari, V., 2021. Hazardous microplastic characteristics and its role as a vector of heavy metal in groundwater and surface water of coastal south India. J. Hazard. Mater. 402 https://doi.org/10.1016/j.jhazmat.2020.123786.

Słowicka, A.M., Ekiel-Jezewska, M.L., Sadlej, K., Wajnryb, E., 2012. Dynamics of fibers in a wide microchannel. J. Chem. Phys. 136 (4), 044904 https://doi.org/10.1063/1.3678852.

Sternberg, H., 1875. Untersuchungen Uber Langen-und Querprofil geschiebe fuhrender Flusse. In: Zeitschrift Für Bauwesen XXV, pp. 483–506.

Toumi, H., Abidli, S., Bejaoui, M., 2019. Microplastics in freshwater environment: the first evaluation in sediments from seven water streams surrounding the lagoon of Bizerte (Northern Tunisia). Environ. Sci. Pollut. Res. https://doi.org/10.1007/s11356-019-04695-0.

Viaroli, S., Lancia, M., Re, V., 2022. Microplastics contamination of groundwater: current evidence and future perspectives. A review. Sci. Total Environ. 824 https://doi.org/10.1016/j.scitotenv.2022.153851.

Waldschläger, K., Schüttrumpf, H., 2020. Infiltration behavior of microplastic particles with different densities, sizes, and shapes-from glass spheres to natural sediments. Environ. Sci. Technol. 54 (15), 9366–9373. https://doi.org/10.1021/acs.est.0c01722.

Wang, C., Zhao, J., Xing, B., 2021b. Environmental source, fate, and toxicity of microplastics. J. Hazard. Mater. 407 https://doi.org/10.1016/j.jhazmat.2020.124357. Elsevier B.V.

Wang, Q., Hernández-Crespo, C., Du, B., Van Hulle, S.W.H., Rousseau, D.P.L., 2021a. Fate and removal of microplastics in unplanted lab-scale vertical flow constructed wetlands. Sci. Total Environ. 778. https://doi.org/10.1016/j.scitotenv.2021.146152.

Wentworth, C.K., 1922. A Scale of Grade and Class Terms for Clastic Sediments.